Determination of Process Parameters for Electron Beam Sintering (EBS)

M. F. Zäh, S. Lutzmann*, M. Kahnert and F. Walchshäusl
iwb Anwenderzentrum Augsburg
*Corresponding author: *iwb* Anwenderzentrum Augsburg, TU München, Beim Glaspalast 5, 86153 Augsburg, Germany, stefan.lutzmann@*iwb*.tum.de

Abstract: Additive Layer Manufacturing (ALM) methods, like Electron Beam Sintering (EBS) constitute an interesting process concerning the production of small series and customised products. However, transient effects occur during processing due to the different physical principles of an electron beam (EB). Thus, process knowledge from similar ALM technologies, for instance Selective Laser Melting, can not be utilised in further developments of EBS. Therefore, a thermal process model including phase and density changes is being formulated and solved using COMSOL Multiphysics 3.4. As a result, the examination of the transient temperature distribution within the process domain leads to the determination of the main process parameters. Current process deficiencies may be eliminated and increasing process stability will be achieved.

Keywords: Additive Layer Manufacturing (ALM), Electron Beam Sintering (EBS), Process Modelling, Thermal Simulation

1. Introduction

The EBS is an Additive Layer Manufacturing (ALM) method for the production of metal parts. Within the process, an electron beam (EB) is utilised in order to selectively solidify a powder layer. Among other advantages, EBS offers fast beam deflection, high beam power density as well as high energy efficiency. However, this technology is also characterised by a complex interaction of various process parameters, such as beam power, powder layer thickness and temperature. The process sequence (lowering the building platform – powder deposition – sintering of powder) is similar to other additive layer manufacturing technologies which are melting powder materials selectively using a laser beam, as shown in Fig. 1.

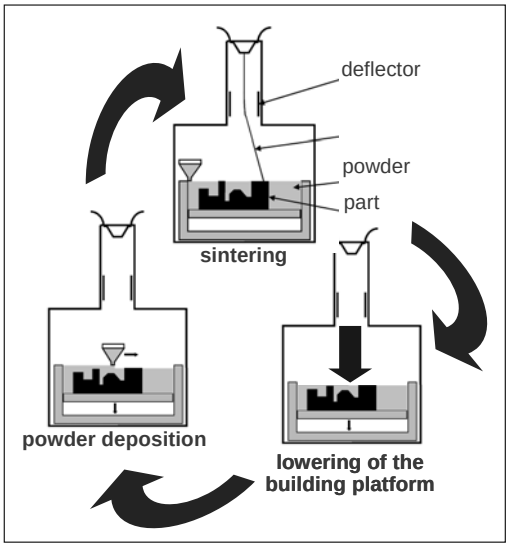

Figure 1: Functional principle of metal processing ALM technologies

First papers with a description of the electron beam as an energy source for direct manufacturing were published in 1992 [1]. In 1997, patents led to the founding of the Swedish company ARCAM AB, which, as an equipment manufacturer, distributes the two systems EBM S12 and A2 [2]. Taminger et al. [3] and Davé [4] suggested the use of wire feed systems to produce metal parts using the electron beam. Another research approach was published by Qui et al. [5]. The *iwb* uses powder materials in order to built complex parts with specific geometric features [6]. A commercial electron beam system developed for joining purposes was modified for the use as an ALM machine. This system is provided by the company *pro-beam AG & Co. KGaA*, which is an equipment manufacturer as well as a contract manufacturer within the field of industrial EB technology.

There is a wide difference between the electron beam and the laser beam process characteristics due to their particular physical principles. As the electrons collide with the powder in the case of the electron beam, negative

charging is transmitted onto the particles. Thus, Coulomb forces arise which lead to a sudden spreading of the complete powder layer. This undesirable effect stops the manufacturing process at once and therefore needs to be avoided by preheating the material. By increasing the powder bed temperature, single particles converge [7] and start to build up an electric conduction towards the grounding building plate. Furthermore, mechanical interconnections develop, keeping the particles in place even in the event of any forces on the powder.

Based on the illustrated spreading of the powder, the EBS process differs by the additional preheating step from laser-based processes. Due to the described physical effects, the selective melting of the powder layer using an EB has to be analysed under the influence of the required preheating step. Furthermore, the electron beam has different characteristics in transmitting energy into the powder material compared to the laser beam. Therefore, a thermal simulation model was set up in order to best represent the real process. The overall objective is to eliminate current process deficiencies and to increase process stability.

2. Theory and Methods

Currently, two major deficiencies in building an EBS part can be identified. First, instabilities in forming an even and smooth layer of solidified material occur. This is often referred to as the "balling"-effect. Second, two consecutive layers tend to separate which is defined as "delamination". Within this paper the balling-effect is being examined in detail.

Balling occurs when the molten material does not wet the underlying substrate plate due to surface tension, which tends to spheroidise the liquid. This results in a rough and bead-shaped surface, obstructing a smooth layer deposition and decreasing the density of the produced part [8]. Given a standard scan pattern, such as bidirectional line x of a square, both process deficiencies are mainly determined by the setting of beam related parameters [9]. Thus, for EBS the following are being investigated in detail: accelerating voltage U_a, beam current I_b, beam spot diameter d_b, hatch distance h, scanning speed v_s, powder layer thickness t_l and preheating temperature υ_p (cf. Fig. 2).

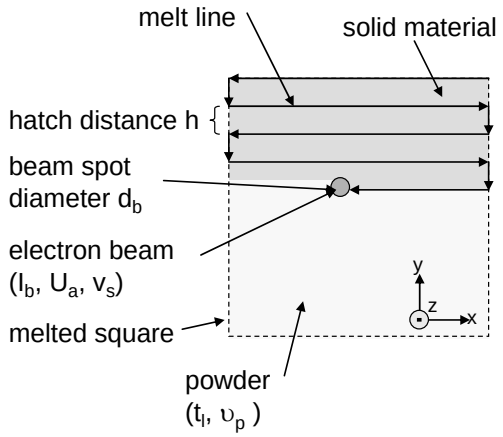

Figure 2: Bidirectional line x scanning of a square

In order to facilitate the problem and to shorten the required time for the calculation of the numerical model, a representative part of molten powder is being extracted from the layer. Thus, this representative volume element is modelled in detail (cf. Fig. 3).

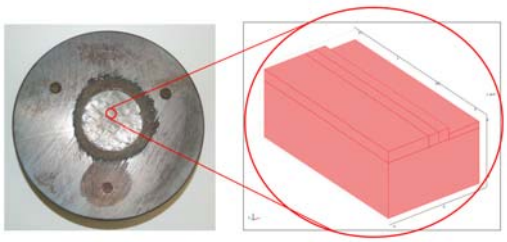

Figure 3: Extracted geometry from the melted layer

The basic principle of the EBS technology is the solidification of metal powder according to the required part cross section. Thus, it is required to achieve a significant temperature increase in the process zone. Therefore, a thermal FEM-model is being formulated and subsequently solved using COMSOL Multi-physics 3.4.

3. Governing Equations

3.1 Heat Conduction Equation

The temperature distribution within the process domain is given by the heat conduction equation:

$$\rho c \frac{\partial \upsilon}{\partial t} = div\left[\lambda \cdot grad\upsilon\right] + \dot{Q} \qquad (1)$$

In the above eq. (1) υ is the temperature, c is the specific heat capacity, ρ is the density and λ is the heat conductivity of the material. The parameter $\dot{Q}$ represents the heat source given by the electron beam penetrating the powder material. According to the specific problem, additional terms or interdependencies must be considered in order to reflect particular loads and boundary conditions.

First, the heat source is three dimensional and transient. It is moving with constant velocity v_s into the x direction. Second, the material properties c, ρ and λ are temperature dependent. Thus, eq. (1) can be rewritten as follows:

$$\frac{\lambda(\upsilon)}{\rho(\upsilon)c(\upsilon)}\left(\frac{\partial^2\upsilon}{\partial x^2}+\frac{\partial^2\upsilon}{\partial y^2}+\frac{\partial^2\upsilon}{\partial z^2}\right)+ \qquad (2)$$
$$+\frac{\dot{Q}(x,y,z,t)}{\rho(\upsilon)c(\upsilon)}=\frac{\partial\upsilon}{\partial t}+v_s\frac{\partial\upsilon}{\partial x}$$

3.2 Heat Source Model

As a required parameter for the adequate modelling of the energy input, a mathematically correct formulation of the powder absorptivity, depending on the penetration depth and the intensity distribution of the electron beam, is necessary. For this reason, the underlying thermo physical model uses a mathematically abstracted heat source with a variable intensity distribution and an adjustable power density as described in the following paragraphs.

Basically, the horizontal intensity distribution I_{xy} can be defined by a Gaussian density function including the standard deviation σ, which can be calculated from experiments determining the beam spot diameter.

$$I_{xy}=\frac{1}{2\pi\sigma^2}e^{-\frac{1}{2\sigma}(x^2+y^2)} \qquad (3)$$

Accordingly, the determination of the vertical intensity distribution I_z is carried out. According to [10], the absorbed power per volume was examined experimentally and subsequently approximated as an intensity function depending on the distance to the surface with the following eq. (4).

$$I_z=\frac{1}{0.75}(-2.25\left(\frac{z}{S}\right)^2+1.5\frac{z}{S}+0.75) \qquad (4)$$

In this formula, S is the absolute penetration depth. That is the perpendicular distance from the part surface where at least 99 % of the electron beam power has already been absorbed by the material.

Thus, the three dimensional heat source can be determined by the superposition of I_{xy} and I_z. Additionally, efficiency values for the beam control η_b and energy conversion at the part surface η_e as well as the electron beam power P_{EB} need to be considered. $\dot{Q}$ can be formulated as follows:

$$\dot{Q}(x,y,z)=-\eta_b\cdot\eta_e\cdot P_{EB} \qquad (5)$$
$$\cdot\frac{4\ln(0,1)}{\pi {d_b}^2 S}e^{\frac{4\ln(0,1)}{{d_b}^2}(x^2+y^2)}\cdot\left(-3\left(\frac{z}{S}\right)^2-2\frac{z}{S}+1\right)$$

However, $\dot{Q}(x,y,z)$ may also be plotted as an isosurface diagram, reflecting the intensity distribution in W/m³ as shown in Fig. 4:

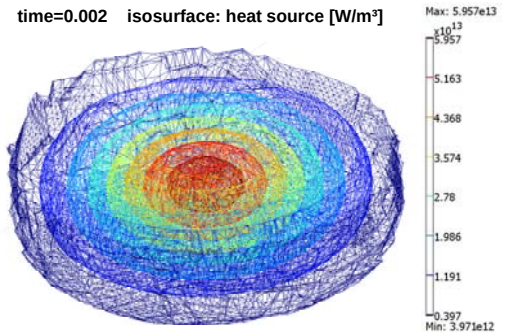

Figure 4: Heat source isosurface plot

The foregoing diagram has been prepared using COMSOL Multiphysics 3.4. The horizontal intensity distribution as well as the vertical decrease of beam power can easily be recognized.

3.3 Boundary and Starting Conditions

In order to represent the given heat conduction problem, boundary and starting conditions need to be considered. Therefore, relevant relations have to be assigned to the boundaries of the extracted geometry in Fig. 3.

During the process, a certain amount of heat Q is lost at the surface of the powder layer by radiation. Thus, the respective equation for the heat flux is given by

$$\dot{Q}=A\cdot\sigma\cdot\varepsilon\cdot\left(\upsilon^4-\upsilon_a^4\right). \qquad (6)$$

The parameter A describes the surface area, σ is the Stefan-Boltzmann-constant ($\sigma=5{,}67\cdot10^{-8}$ W/(m²K⁴)), υ_a is the ambient temperature set to

298,15 K and ε equals the emissivity, which is temperature dependent and can be taken from [11] (cf. Table 1).

Another important energy flux through the vertical boundaries as well as through the undersurface of the examined geometry is provided by heat conduction. Hence, there is a direct contact between those boundaries and the powder and bulk material in the surrounding area. Consequently, the heat flux density at the inner side (index „i“) of the boundary equals the one at the outer side (index „o“) of the boundary:

$$\lambda^{(i)}\left(\frac{\partial \upsilon^{(i)}}{\partial n}\right)_b = \lambda^{(o)}\left(\frac{\partial \upsilon^{(o)}}{\partial n}\right)_b \qquad (7)$$

That implies that the temperatures of adjacent domains are equal but at the same time, different temperature gradients are being reached depending on the respective values of the heat conductivity λ.

Finally, a starting condition concerning the temperature within the process domain needs to be defined. As mentioned in section 1, the powder is being preheated prior to the actual sintering process. As measured by thermocouple devices, the temperature at the end of the preheating step is uniform. Thus, at the time t=0, υ_p equals 1353 K.

3.4 Material Properties

The powder material consists of a multitude of particles of different sizes and geometries. Modelling of a huge number of single particles would result in an enormous computing time [12]. Therefore, examinations [13] have shown that in thermal calculations, metal powder can be considered as a continuum. Different from metal powders for ALM, the temperature dependent values of c, ρ and λ for bulk material can be extracted from a number of publicly available literature, e.g. [14]. In order to determine the respective powder values, models for the calculation can be found in the literature. In adopting the values of the considered conditions, the distribution of the required material properties can be determined. However, those properties can either be taken from literature or be calculated from the respective bulk material values. In the presented work, stainless steel 1.4404 has been used for the evaluation.

The emissivity of iron based powder of the identical particle size was calculated by [11] and validated by experimental series (cf. Table 1).

T [K]	333	481	569	680	755	1208	1396
ε	0,78	0,8	0,81	0,83	0,86	0,94	0,98

Table 1: Temperature dependent values for the emissivity of powder

The heat conductivity of powders differs significantly from the respective values of bulk material. Furthermore, this property of powder beds is also of special relevance in heat exchangers. Therefore, various examinations have been dealing with its modelling and calculation, such as [12,13].

The so called Zehner/Bauer/Schlünder model [14] has been used to calculate the effective heat conductivity of the examined powder below solidus temperature (cf. Fig. 5). Within this range, the values vary between 0.03 W/(mK) and 0.1 W/(mK). From solidus temperature (1658 K) to liquidus temperature (1699 K), sintering takes place and the powder begins to adopt bulk material properties.

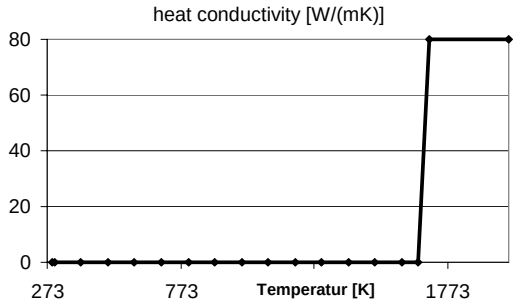

Figure 5: Heat conductivity of the powder

The distribution of the material density is similar to that of the heat conductivity as the material is melting and thus, shrinking towards its final bulk density. The heat capacity of powder is equal to that of its respective bulk material and can be taken from [14].

4. Numerical Model

Analytically derived results are applied in order to investigate the required beam energy for a process stable solidification of metal layers in EBS. Within the numerical simulation, a thermal model with characteristic material values is used. Both powder specific parameters and solid

material parameters are assigned to the geometrical information.

According to [15], the predefined zone of the so called *melt line* is meshed accurately (cf. Fig. 6) in consideration of the expected temperature gradients induced by the energy input.

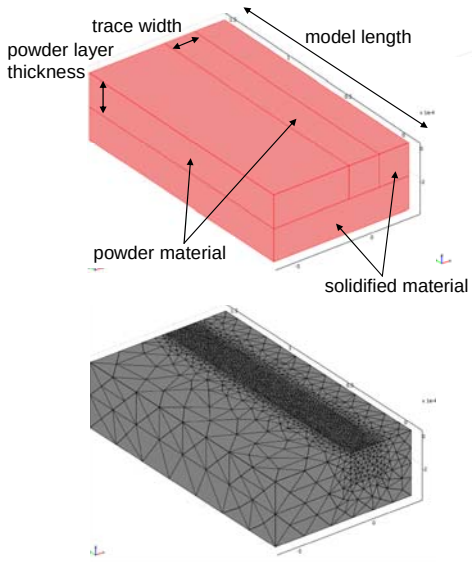

Figure 6: Simulation model (left: geometrical set-up; right: mesh)

Referring to the numerical model, the simulation is performed in dependence of the scanning speed and the inserted electron beam power. Parameters during the simulation are varied under the assumption of sufficiently reproducing the real experiment, which can be characterised by the following parameters:

electron beam (EB) radius	$1.0 \cdot 10^{-04}$ m
EB penetration depth	$6.2 \cdot 10^{-05}$ m
trace width	$2.0 \cdot 10^{-04}$ m
model length	$2.0 \cdot 10^{-03}$ m
powder layer thickness	$1.0 \cdot 10^{-04}$ m

Subsequent to the calculation, the achieved transient temperature distribution is evaluated. The special objective consists of analyzing the transient temperature distribution within the process domain (cf. Fig. 7).

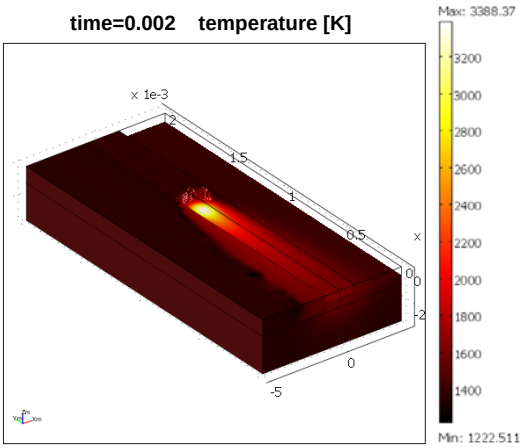

Figure 7: Temperature distribution within the process domain

5. Simulation Results and Discussion

In order to achieve a homogeneous melted layer, two different criteria have to be met. First, the temperatures within the powder layer have to be at least as high as the melting temperature of the material. Second, the size and shape of the melt pool exhibits an important parameter in avoiding balling [8]. Therefore, different parameter settings had been evaluated. After several simulation runs, process parameters according to Table 2 could be defined and used for the build-up of several layers of stainless steel (cf. Fig. 3).

Process parameter	Variable	Value
accelerating voltage	U_a	100 kV
beam current	I_b	1 mA
beam spot diameter	d_b	200 µm
layer thickness	t_l	100 µm
preheating temperature	υ_p	1353 K
scan speed	v_s	0.1 m/s
hatch distance	h	0.1 mm

Table 2: Parameter setting for the evaluation

A point at an arbitrary position within the *melt line* was chosen for evaluation (cf. Fig. 8). The temperature on the surface and $1 \cdot 10^{-4}$ m below the surface exceeds the melting temperature of 1699 K. The third position, $1 \cdot 10^{-4}$ m below the powder layer is also being heated by the electron beam after a short delay.

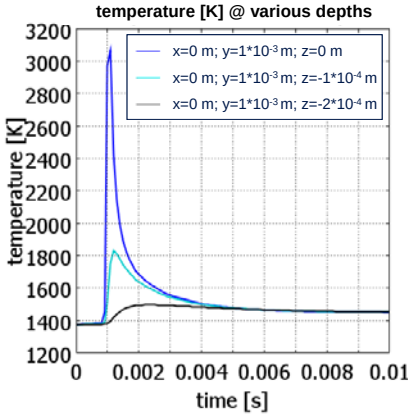

Figure 8: Time dependent temperature distribution of three points in the melt line

As mentioned earlier, the size and shape of the melt pool is another relevant criterion. Examinations concerning selective laser melting have shown that the length to width ratio of the melt pool may not exceed 2.1 in order to avoid the balling effect [8]. Thus, COMSOL Multi-physics 3.4 was used in order to indicate temperatures in the process domain greater than 1699 K (cf. Fig. 9).

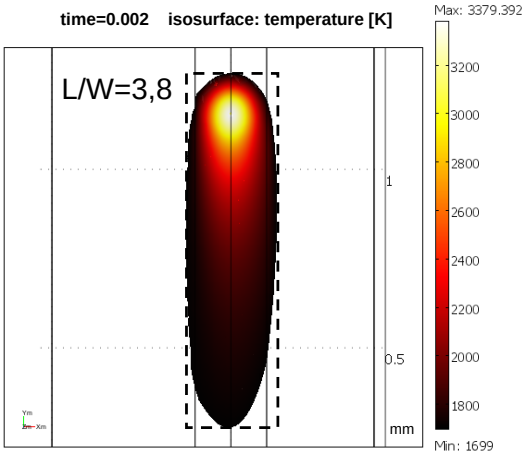

Figure 9: Size and shape of the melt pool

As it can be seen, the length to width ratio with the given parameters is 3.8. In contrast to the results in laser beam melting, this also leads to acceptable results in EBS. A possible explanation is that the preheating temperature in EBS is significantly higher than in laser beam assisted processes. Thus, temperature gradients to the surrounding material are reduced and therefore, the molten material tends less to form into a spherical shape. Additionally, electron beam sintering takes place under vacuum which leads to a different surface tension of the molten phase. Hence, balling is not as likely to happen.

6. Conclusion

In the presented paper, the basic principles of EBS were introduced. As the utilised electron beam's physical properties differ significantly from those of laser beams, efforts where taken in order to investigate the effect on the interaction with metal powder. Therefore, a thermal simulation model was set up by the formulation of a mathematically abstracted heat source, based on the general heat conduction equation with a moving energy source. Based on the development of the EBS technology, various combinations of process parameters had been applied within the simulation in order to determine the temperature as well as the size and shape of the melt pool. The results were compared with real experiments. It was noticed that these results concur largely with the simulation. In the future, experimental simulation series can be conducted before the actual build-up of the parts in order to investigate the correct values of the applied parameters. Thus, time and effort for building jobs can be saved by prior simulation runs.

Certain challenges still remain. The simulation model needs to be improved concerning the size of the scanned pattern in order to better reflect real process conditions. However, a reasonable balance of computation time and significance of the obtained results must be considered.

8. References

[1] Patent WO 1994026446 A1 Method and Device for producing Three-dimensional Bodies (24.11.1994). Larson, R. Pr.: SE 9301647 Larson, R.: Method and Device for producing Three-dimensional Bodies.

[2] ARCAM: APPLICATIONS. <http://www.arcam.com/applications/index.asp> (June 18th, 2007)

[3] Taminger, K. M. B.; Hafley, R. A.: Characterization of 2219 Aluminium Produced by Electron Beam Freeform Fabrication. In: Bourell, D. L. et al. (Editors): Solid Freeform Fabrication Symposium Proceed-

ings 13; Austin,Texas/USA; August 5 - 7, 2002. The University of Texas at Austin 2002, pp. 482-489.

[4] Dave, V. R.: Electron Beam Assisted Materials Fabrication. Diss. Massachusetts Institute of Technology (1995).

[5] Qi, H. B.; Yan, Y. N.; Lin, F.; He, W.; Zhang, R. J.: Direct metal part forming of 316L stainless steel powder by electron beam selective melting. Proceedings of the Institution of Mechanical Engineers -- Part B -- Engineering Manufacture 202 (2006) 11, pp. 1845-1853.

[6] Meindl, M.: Beitrag zur Entwicklung generativer Fertigungsverfahren für das Rapid Manufacturing. Diss. Technische Universität München (2004). München: Utz 2005. (*iwb* Forschungsberichte 187).

[7] German, R. M.: Sintering theory and practice. New York: Wiley 1996.

[8] Gusarov, A. V.; Yadroitsev, I.; Betrand, P.; Smurov, I.: Heat transfer modelling and stability analysis of selective laser melting. Applied Surface Science 254 (2007), pp. 975-979.

[9] Kruth, J. P.; Froyen, L.; Vaerenbergh, J. V.; Rombouts, M.; Lauwers, B.: Selective laser melting of iron-based powder. Materials Processing Technology 149 (2004), pp. 612 - 622.

[10] Heinrich, H.: Theoretische und experimentelle Untersuchungen zur Bestimmung der Intensitätsverteilung im Strahlungsfeld von Elektronenbeschleunigern und der Dosisverteilung in elektronenbestrahlten Material. Diss. Akademie der Wissenschaften (1973).

[11] Sih, S. S.; Barlow, J. W.: Emissivity of Powder Beds. In: Marcus, H. L. et al. (Editors): Solid Freeform Fabrication Symposium Proceedings 6; Austin, Texas/ USA; August 7 - 9. The University of Texas at Austin 1995, pp. 402-408.

[12] Wagner, C. A.: Untersuchungen zum selektiven Lasersintern von Metallen. Aachen: Shaker 2003. (Berichte aus der Produktionstechnik 2003, 11).

[13] Schlünder, E.-U.; Tsotsas, E.: Wärmeübertragung in Festbetten, durchmischten Schüttgütern und Wirbelschichten : 33 Tabellen. Stuttgart: Thieme 1988.

[14] Verein Deutscher Ingenieure; Gesellschaft Verfahrenstechnik und Chemieingenieurwesen: VDI-Wärmeatlas: Berechnungsblätter für den Wärmeübergang. Berlin: Springer 2002.

[15] Over, C.: Generative Fertigung von Bauteilen aus Werkzeugstahl X38CrMoV5-1 und Titan TiAl6V4 mit "Selective Laser Melting". Diss. Aachen: Shaker: RWTH Aachen 2003.